Observation of strong coupling through transmission modification of a cavity-coupled photonic crystal waveguide

R. Bose,[1,2,3] D. Sridharan,[1,2,3] G. S. Solomon,[2,3] and E. Waks[1,2,3]

[1]*Department of Electrical Engineering and Institute for Research in Electronics and Applied Physics, University of Maryland, College Park, Maryland 20742, USA*
[2]*Joint Quantum Institute, University of Maryland, College Park, Maryland 20742, USA*
[3]*National Institute of Standards and Technology, Gaithersburg, Maryland, USA*

Abstract: We investigate strong coupling between a single quantum dot (QD) and photonic crystal cavity through transmission modification of an evanescently coupled waveguide. Strong coupling is observed through modification of both the cavity scattering spectrum and waveguide transmission. We achieve an overall *Q* of 5800 and an exciton-photon coupling strength of 21 GHz for this integrated cavity-waveguide structure. The transmission contrast for the bare cavity mode is measured to be 24%. These results represent important progress towards integrated cavity quantum electrodynamics using a planar photonic architecture.

OCIS codes: (270.5580) Quantum Electrodynamics; (130.3120) Integrated optics devices.

References and links

1. Y. Akahane, T. Asano, B. S. Song, and S. Noda, "High-Q photonic nanocavity in a two-dimensional photonic crystal," Nature **425**(6961), 944–947 (2003).
2. Y. Akahane, T. Asano, B. S. Song, and S. Noda, "Fine-tuned high-Q photonic-crystal nanocavity," Opt. Express **13**(4), 1202–1214 (2005).
3. B.-S. Song, S. Noda, T. Asano, and Y. Akahane, "Ultra-high-Q photonic double-heterostructure nanocavity," Nat. Mater. **4**(3), 207–210 (2005).
4. M. Notomi, T. Tanabe, A. Shinya, E. Kuramochi, H. Taniyama, S. Mitsugi, and M. Morita, "Nonlinear and adiabatic control of high-Q photonic crystal nanocavities," Opt. Express **15**(26), 17458–17481 (2007).
5. T. Yamamoto, M. Notomi, H. Taniyama, E. Kuramochi, Y. Yoshikawa, Y. Torii, and T. Kuga, "Design of a high-Q air-slot cavity based on a width-modulated line-defect in a photonic crystal slab," Opt. Express **16**(18), 13809–13817 (2008).
6. T. Yoshie, A. Scherer, J. Hendrickson, G. Khitrova, H. M. Gibbs, G. Rupper, C. Ell, O. B. Shchekin, and D. G. Deppe, "Vacuum Rabi splitting with a single quantum dot in a photonic crystal nanocavity," Nature **432**(7014), 200–203 (2004).
7. K. Hennessy, A. Badolato, M. Winger, D. Gerace, M. Atatüre, S. Gulde, S. Fält, E. L. Hu, and A. Imamoğlu, "Quantum nature of a strongly coupled single quantum dot-cavity system," Nature **445**(7130), 896–899 (2007).
8. D. Englund, A. Faraon, I. Fushman, N. Stoltz, P. Petroff, and J. Vucković, "Controlling cavity reflectivity with a single quantum dot," Nature **450**(7171), 857–861 (2007).
9. Y. Ota, N. Kumagai, S. Ohkouchi, M. Shirane, M. Nomura, S. Ishida, S. Iwamoto, S. Yorozu, and Y. Arakawa, "Investigation of the Spectral Triplet in Strongly Coupled Quantum Dot Nanocavity System," Appl. Phys. Express **2**(12), 122301 (2009).
10. A. Badolato, M. Winger, K. J. Hennessy, E. L. Hu, and A. Imamoglu, "Cavity QED effects with single quantum dots," C. R. Phys. **9**(8), 850–856 (2008).
11. F. S. F. Brossard, X. L. Xu, D. A. Williams, M. Hadjipanayi, M. Hugues, M. Hopkinson, X. Wang, and R. A. Taylor, "Strongly coupled single quantum dot in a photonic crystal waveguide cavity," Appl. Phys. Lett. **97**(11), 111101 (2010).
12. I. Fushman, D. Englund, A. Faraon, N. Stoltz, P. Petroff, and J. Vuckovic, "Controlled phase shifts with a single quantum dot," Science **320**(5877), 769–772 (2008).
13. I. Fushman, "Quantum dots in photonic crystals: From quantum information processing to single photon nonlinear optics," Ph.D. Dissertation, Stanford Univ., 2009.
14. A. Imamoğlu, D. D. Awschalom, G. Burkard, D. P. DiVincenzo, D. Loss, M. Sherwin, and A. Small, "Quantum Information Processing Using Quantum Dot Spins and Cavity QED," Phys. Rev. Lett. **83**(20), 4204–4207 (1999).

#141797 - $15.00 USD Received 27 Jan 2011; accepted 27 Feb 2011; published 8 Mar 2011

Report Documentation Page

Form Approved
OMB No. 0704-0188

1. REPORT DATE	2. REPORT TYPE	3. DATES COVERED
JAN 2011		**00-00-2011 to 00-00-2011**

4. TITLE AND SUBTITLE	5a. CONTRACT NUMBER
Observation of strong coupling through transmission modification of a cavity-coupled photonic crystal waveguide	5b. GRANT NUMBER
	5c. PROGRAM ELEMENT NUMBER
6. AUTHOR(S)	5d. PROJECT NUMBER
	5e. TASK NUMBER
	5f. WORK UNIT NUMBER
7. PERFORMING ORGANIZATION NAME(S) AND ADDRESS(ES) **University of Maryland,Department of Electrical Engineering and,Institute for Research in Electronics and Applied Physics,College Park,MD,20742**	8. PERFORMING ORGANIZATION REPORT NUMBER
9. SPONSORING/MONITORING AGENCY NAME(S) AND ADDRESS(ES)	10. SPONSOR/MONITOR'S ACRONYM(S)
	11. SPONSOR/MONITOR'S REPORT NUMBER(S)

12. DISTRIBUTION/AVAILABILITY STATEMENT
Approved for public release; distribution unlimited

13. SUPPLEMENTARY NOTES

14. ABSTRACT

We investigate strong coupling between a single quantum dot (QD) and photonic crystal cavity through transmission modification of an evanescently coupled waveguide. Strong coupling is observed through modification of both the cavity scattering spectrum and waveguide transmission. We achieve an overall Q of 5800 and an exciton-photon coupling strength of 21 GHz for this integrated cavity-waveguide structure. The transmission contrast for the bare cavity mode is measured to be 24%. These results represent important progress towards integrated cavity quantum electrodynamics using a planar photonic architecture.

15. SUBJECT TERMS

16. SECURITY CLASSIFICATION OF:			17. LIMITATION OF ABSTRACT	18. NUMBER OF PAGES	19a. NAME OF RESPONSIBLE PERSON
a. REPORT **unclassified**	b. ABSTRACT **unclassified**	c. THIS PAGE **unclassified**	**Same as Report (SAR)**	**12**	

15. M. Winger, A. Badolato, K. J. Hennessy, E. L. Hu, and A. Imamoğlu, "Quantum dot spectroscopy using cavity quantum electrodynamics," Phys. Rev. Lett. **101**(22), 226808 (2008).
16. Y. Akahane, T. Asano, B.-S. Song, and S. Noda, "Fine-tuned high-Q photonic-crystal nanocavity," Opt. Express **13**(4), 1202–1214 (2005).
17. Y. A. Vlasov, M. O'Boyle, H. F. Hamann, and S. J. McNab, "Active control of slow light on a chip with photonic crystal waveguides," Nature **438**(7064), 65–69 (2005).
18. S. McNab, N. Moll, and Y. Vlasov, "Ultra-low loss photonic integrated circuit with membrane-type photonic crystal waveguides," Opt. Express **11**(22), 2927–2939 (2003).
19. E. Waks, and J. Vuckovic, "Coupled mode theory for photonic crystal cavity-waveguide interaction," Opt. Express **13**(13), 5064–5073 (2005).
20. E. Waks, and J. Vuckovic, "Dipole induced transparency in drop-filter cavity-waveguide systems," Phys. Rev. Lett. **96**(15), 153601 (2006).
21. D. Sridharan, and E. Waks, "Generating entanglement between quantum dots with different resonant frequencies based on dipole-induced transparency," Phys. Rev. A **78**(5), 052321 (2008).
22. L. M. Duan, M. D. Lukin, J. I. Cirac, and P. Zoller, "Long-distance quantum communication with atomic ensembles and linear optics," Nature **414**(6862), 413–418 (2001).
23. L. Jiang, J. M. Taylor, K. Nemoto, W. J. Munro, R. Van Meter, and M. D. Lukin, "Quantum repeater with encoding," Phys. Rev. A **79**(3), 032325 (2009).
24. H. J. Briegel, W. Dür, J. Cirac, and P. Zoller, "Quantum Repeaters: The Role of Imperfect Local Operations in Quantum Communication," Phys. Rev. Lett. **81**(26), 5932–5935 (1998).
25. L. M. Duan, and R. Raussendorf, "Efficient quantum computation with probabilistic quantum gates," Phys. Rev. Lett. **95**(8), 080503 (2005).
26. X. Yang, M. Yu, D.-L. Kwong, and C. W. Wong, "All-optical analog to electromagnetically induced transparency in multiple coupled photonic crystal cavities," Phys. Rev. Lett. **102**(17), 173902 (2009).
27. A. Faraon, I. Fushman, D. Englund, N. Stoltz, P. Petroff, and J. Vucković, "Dipole induced transparency in waveguide coupled photonic crystal cavities," Opt. Express **16**(16), 12154–12162 (2008).
28. D. F. Walls, and G. J. Millburn, Quantum Optics (Springer, 2008).
29. S. Hughes, and H. Kamada, "Single-quantum-dot strong coupling in a semiconductor photonic crystal nanocavity side coupled to a waveguide," Phys. Rev. B **70**(19), 195313 (2004).
30. J. Pan, S. Sandhu, Y. Huo, N. Stuhrmann, M. L. Povinelli, J. S. Harris, M. M. Fejer, and S. Fan, "Experimental demonstration of an all-optical analogue to the superradiance effect in an on-chip photonic crystal resonator system," Phys. Rev. B **81**(4), 041101 (2010).
31. J.-T. Shen, and S. Fan, "Theory of single-photon transport in a single-mode waveguide. I. Coupling to a cavity containing a two-level atom," Phys. Rev. A **79**(2), 023837 (2009).
32. A. J. Hudson, R. M. Stevenson, A. J. Bennett, R. J. Young, C. A. Nicoll, P. Atkinson, K. Cooper, D. A. Ritchie, and A. J. Shields, "Coherence of an entangled exciton-photon state," Phys. Rev. Lett. **99**(26), 266802 (2007).
33. E. Waks, and D. Sridharan, "Cavity QED treatment of interactions between a metal nanoparticle and a dipole emitter," Phys. Rev. A **82**(4), 043845 (2010).
34. A. Faraon, E. Waks, D. Englund, I. Fushman, and J. Vuckovic, "Efficient photonic crystal cavity-waveguide couplers," Appl. Phys. Lett. **90**(7), 073102 (2007).

1. Introduction

Semiconductor quantum dots (QDs) coupled to photonic crystal structures provide a promising physical platform for studying strong atom-light interactions. Photonic crystal cavities exhibit both high quality factors (Q) and small mode volumes [1–5] enabling the study of cavity quantum electrodynamics in the strong coupling regime [6–11]. Strong coupling has important applications in the areas of nonlinear optics [8,12], quantum information processing [13,14], and spectroscopy [15].

Another advantage of photonic crystal structures is that they provide a method to integrate a large number of optical components in a compact device. Such devices can be used to implement complex photonic circuits where individual components communicate over optical channels. These channels can be realized using line-defect waveguides [16,17] that can transport light with low optical losses [17,18] as well as slow group velocities creating strong interaction with other optical components over short distances [17,19]. By combining waveguides with optical cavities that are strongly coupled to quantum dots it becomes possible to create quantum interactions between the spatially separated QDs using light as a quantum interface [20–23], which forms the basis for universal quantum computation and quantum networking [24,25].

In order to take full advantage of the ability of photonic crystals to create integration we need to develop device structures where the cavity can be driven and can also emit into an

#141797 - $15.00 USD Received 27 Jan 2011; accepted 27 Feb 2011; published 8 Mar 2011

integrated waveguide. Such devices have been routinely fabricated in passive silicon structures that do not contain QDs and used to probe the cavity properties [16,26]. To incorporate quantum dots, however, it is necessary to work in gallium arsenide (GaAs) material systems which suffer from higher losses and lower cavity *Q*, particularly in the near infrared wavelengths. The introduction of the waveguide causes a critical reduction in the resonator *Q* due to the new channel for optical losses, making it difficult to achieve the strong coupling regime. For this reason previous investigations of coupled cavity-QD systems through planar waveguide transmission have been performed in the weak coupling regime [27].

In this work, we study strong coupling between an indium arsenide (InAs) QD and a photonic crystal cavity using a planar waveguide transmission measurement rather than photoluminescence. We design and fabricate a photonic crystal structure composed of a cavity evanescently coupled to a row defect waveguide, with a single QD resonantly coupled to the cavity mode. The cavity has a sufficiently high cavity *Q* to achieve strong coupling, while also maintaining sufficiently strong coupling to the waveguide to achieve a 24% transmission contrast. Strong coupling is observed by driving the cavity-QD system near resonance through the waveguide and measuring the waveguide transmission and cavity scattering spectrum. This approach provides a simple way to separate the pump and cavity signal in order to coherently measure the strongly coupled system. The results represent an important step towards development of integrated planar device structures where waveguides are used to create an optical interface between spatially separated QDs.

2. Device Design

The device structure used in this work is shown schematically in Fig. 1a. The device is comprised of a photonic crystal cavity evanescently coupled to a row defect waveguide. The cavity design is a three-hole linear defect (L3) cavity with three-hole tuning [16]. As shown in Fig. 1a, the holes A, B, and C adjacent to the cavity are shifted by 0.176*a*, 0.024*a* and 0.176*a* respectively, where *a* is the lattice constant, in order to improve the overall *Q*. The lattice parameter *a* is set to be 240 nm, the diameter of the air holes is set to 140 nm, and the photonic crystal slab thickness is set to be 160 nm. The line defect waveguide is formed by removing a row of holes below the cavity.

The dispersion diagram for the transverse electric (TE) modes of the bare photonic crystal waveguide (no cavity) is shown in Fig. 1b. Modes are plotted as a function of the in-plane crystal momentum k_x (in units of a/π) and mode frequency (in units of a/λ), while the solid red line represents the light line of the slab waveguide. The waveguide dispersion was calculated using finite difference time domain (FDTD) simulations (Lumerical FDTD). The band structure exhibits a TE bandgap between ω = 0.232 and 0.287. Below the light line, the even waveguide mode has a passband in the frequency range of $\omega \in [0.241, 0.262]$. At the edge of the Brillioun zone, the waveguide exhibits a slow group velocity region at a frequency of ω = 0.241. In order to couple the cavity strongly to the waveguide mode, it is important that the cavity resonance overlaps with the slow group velocity region of the waveguide, where the enhanced waveguide density of states can significantly increase the coupling between the two systems [19]. To achieve this condition, the size of the holes above and below the row defect is reduced by 4% relative to the other holes in the photonic crystal. Reducing these hole sizes serves to pull the band edge of the waveguide to lower energies so that it better overlaps with the cavity resonance. Using this device design we calculate the properties of the cavity by placing a point source dipole emitter with a broad spectral response at the high electrical field region of the cavity mode. From this calculation we determine the theoretical cavity *Q* to be 10,000, and the cavity resonance frequency to be 0.245. Figure 1c shows the calculated $\mathbf{H}_z$ mode profile of the cavity, which exhibits a clear coupling to the waveguide mode.

#141797 - $15.00 USD Received 27 Jan 2011; accepted 27 Feb 2011; published 8 Mar 2011

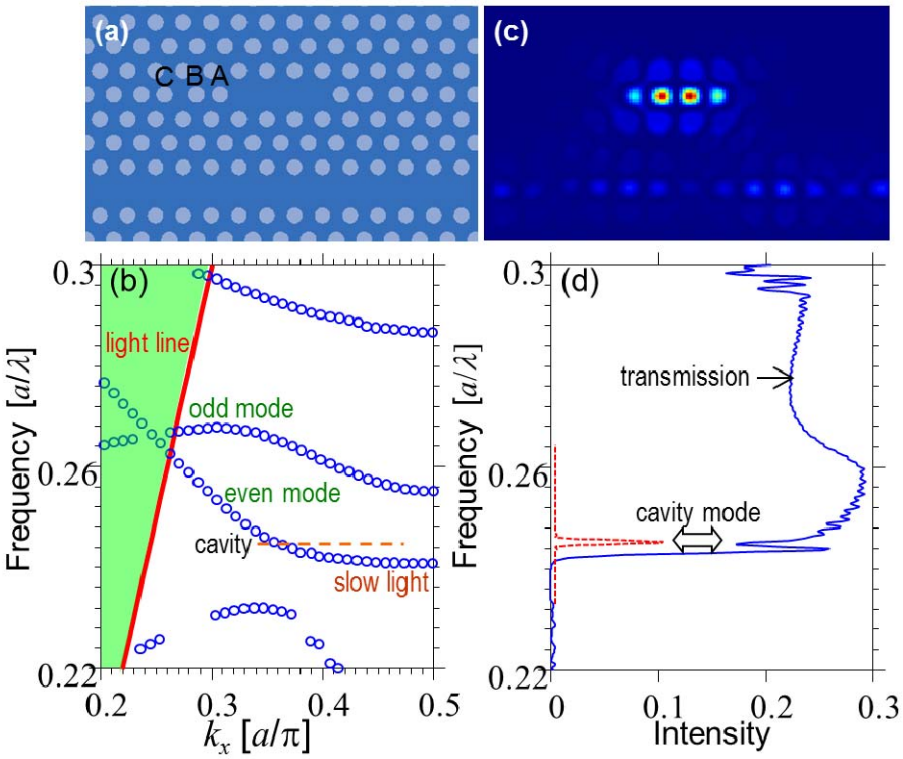

Fig. 1. (a) Schematic of simulated structure. (b) Simulated photonic band structure for photonic crystal waveguide with waveguide-edge holes reduced by 4%. The light line is shown by solid red line. (c) Field profile $(\mathbf{H})_z$ of computed cavity-field mode, shown over the simulation region in (a). (d) Simulated transmission spectrum (solid blue line), along with the spectral response of the fundamental cavity mode (dashed red line) computed using a broadband source inside the cavity.

Figure 1d shows the calculated transmission of the waveguide (solid blue line) in the device structure shown in Fig. 1a as a function of optical frequency in units of a/λ. The waveguide transmission is calculated by placing a broadband point source at the mid-plane of the photonic crystal slab at one end of the waveguide and calculating the transmitted power at the other end. The transmission of the waveguide exhibits a broad pass band that cuts off sharply at a normalized frequency of 0.241, as expected from the waveguide dispersion diagram. The sharp cutoff denotes the waveguide stop band. An anti-resonance in the transmission spectrum is observed at the cavity frequency of 0.245 with a corresponding 29% reduction in transmission. The anti-resonance is due to both reflection and out-of-plane scattering from the cavity mode. In addition to the waveguide transmission, we also plot the calculated cavity spectral response when excited by a broadband point dipole source (red dashed line). These spectra show that the cavity spectrum is in agreement with the anti-resonance of the waveguide transmission, and also overlaps the slow group velocity regime of the waveguide mode.

3. Fabrication

The initial wafer for the device fabrication, grown by molecular-beam epitaxy, was composed of a 160-nm GaAs membrane with an InAs QD layer grown at the center (with QD density of approximately 10 μm^{-2}), on a 1-μm thick sacrificial layer of aluminum gallium arsenide ($Al_{0.78}Ga_{0.22}As$). Photonic crystals were defined on the GaAs membrane using electron-beam lithography, followed by chlorine-based inductively coupled plasma dry etching. Selective

#141797 - $15.00 USD Received 27 Jan 2011; accepted 27 Feb 2011; published 8 Mar 2011

wet etching was then used to remove the sacrificial AlGaAs layer, resulting in a free-standing GaAs membrane. Figure 2a shows a scanning electron micrograph (SEM) of a fabricated device, where the design parameters are identical to those simulated in Section 2. The total device length was set to 80*a*, which is sufficiently long to optically isolate the cavity from the input and output facets of the device. In order to inject and collect light from the waveguide in the out-of-plane direction, we employ grating couplers at the two ends of the waveguide, as originally proposed and demonstrated by Faraon *et. al* [27]. These couplers have been shown to couple as much as 50% of the light in the out-of-plane direction. A close-up of the cavity interaction region and grating coupler are shown in panels b and c respectively.

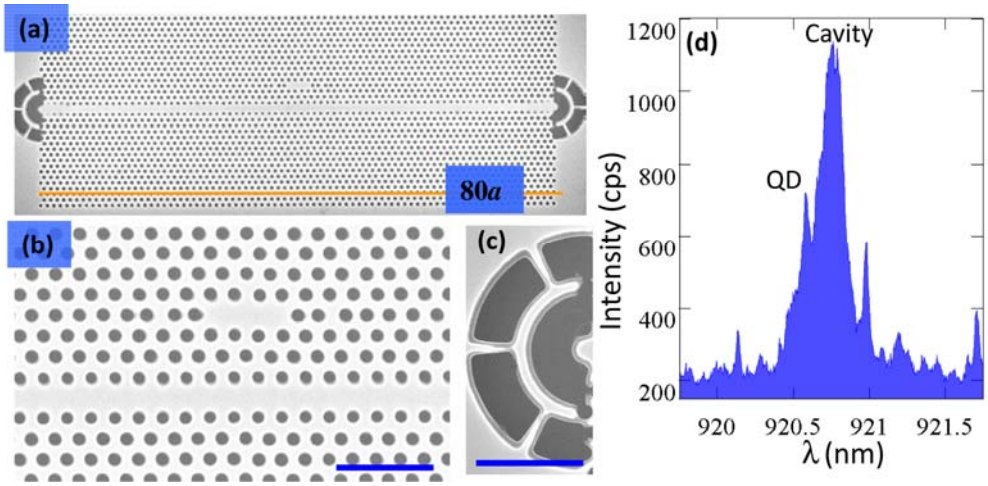

Fig. 2a. (a) Scanning electron micrograph showing a typical fabricated device. (b) Closeup of the cavity-waveguide region, showing the design adjustments for optimal performance. (c) Closeup of the input grating coupler. Scale bars in (b) & (c) correspond to 1 μm. (d) Low power (5 μW) above-band excitation of the cavity.

4. Experimental Setup and Device Characterization

The sample was mounted in a liquid helium cryostat with temperature varying between 15 K and 35 K. Three light sources were used in the experiments. A Ti:Sapphire laser operating in continuous wave mode was used for above-band out-of-plane excitation in order to measure the photoluminescence properties of the device. A broadband light emitting diode operating between 900 and 1000 nm was used to investigate the transmission and scattering spectrum of the device in the weak field limit by exciting through the input grating and observing radiation at the cavity or at the outcoupler at low incident photon flux. Finally, a tunable external cavity diode laser (New Focus Velocity) enabled us to probe the system with high power narrowband field for power-dependent near-resonant excitation experiments. A polarization setup consisting of a half waveplate and polarizing beamsplitter was used to match the excitation source with the polarization of the waveguide mode. Emission was collected by a confocal microscope setup using a 0.7 NA objective lens, followed by spatial filtering to isolate the scatter from either the cavity or output coupler. The collected emission was then measured by a grating spectrometer with a wavelength resolution of 0.02 nm.

#141797 - $15.00 USD Received 27 Jan 2011; accepted 27 Feb 2011; published 8 Mar 2011

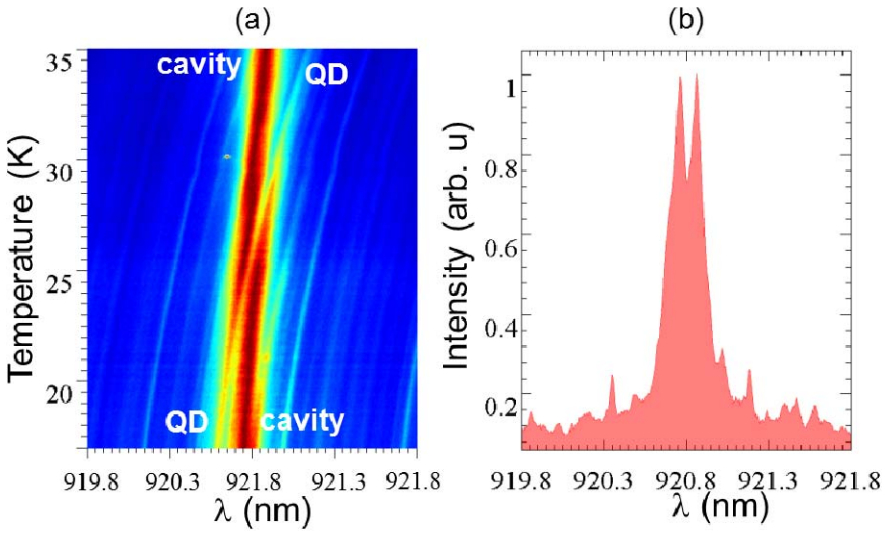

Fig. 3. (a) Temperature scan of the cavity QD system using above-band (780 nm) excitation showing an anti-crossing around 27 K due to strong coupling. (b) Cavity spectrum at the strong coupling point using low power excitation, with a measured splitting of 0.09 nm between the polariton peaks.

Devices were initially characterized using above-band (780 nm) excitation. Figure 2d shows the photoluminescence spectrum of the cavity when directly excited by the above-band pump. The spectrum shows a bright emission peak from the cavity mode at 920 nm, along with several nearby QDs. The QD we focus on in this work is labeled in the spectrum. By fitting the cavity to a Lorentzian function we determine the cavity Q to be 5800, which corresponds to a cavity decay rate of κ = 56 GHz. In order to tune the QD onto the cavity resonance the temperature of the device was tuned from 17 K to 35 K. The photoluminescence spectrum as a function of sample temperature is show in Fig. 3a. Near 27 K, the QD becomes resonant with the cavity mode resulting in significant enhancement of the cavity emission as well as a clear anti-crossing behavior, indicating that the QD and cavity are in the strong coupling regime. The minimum separation between the two polariton modes of the strongly coupled system occurs at a temperature of 27K. The cavity spectrum at this temperature is plotted in Fig. 3b. This spectrum is fit to a double Lorentzian spectrum in order to calculate the vacuum Rabi splitting (VRS) which is given by 0.09 nm and corresponds to a frequency splitting of Δ = 31.5 GHz. From the vacuum Rabi splitting we calculate the QD-cavity coupling strength g using the relation [7]:

$$2g \approx \sqrt{\Delta^2 + (\kappa - \gamma)^2 / 4}, \qquad (1)$$

where $\gamma/2\pi$ = 0.1 GHz is the QD spontaneous emission rate [8]. From the above equation we determine that g = 21 GHz, which satisfies the strong coupling condition $g > \kappa/4$ for κ = 56 GHz.

#141797 - $15.00 USD Received 27 Jan 2011; accepted 27 Feb 2011; published 8 Mar 2011

5. Weak field transmission and scattering measurements

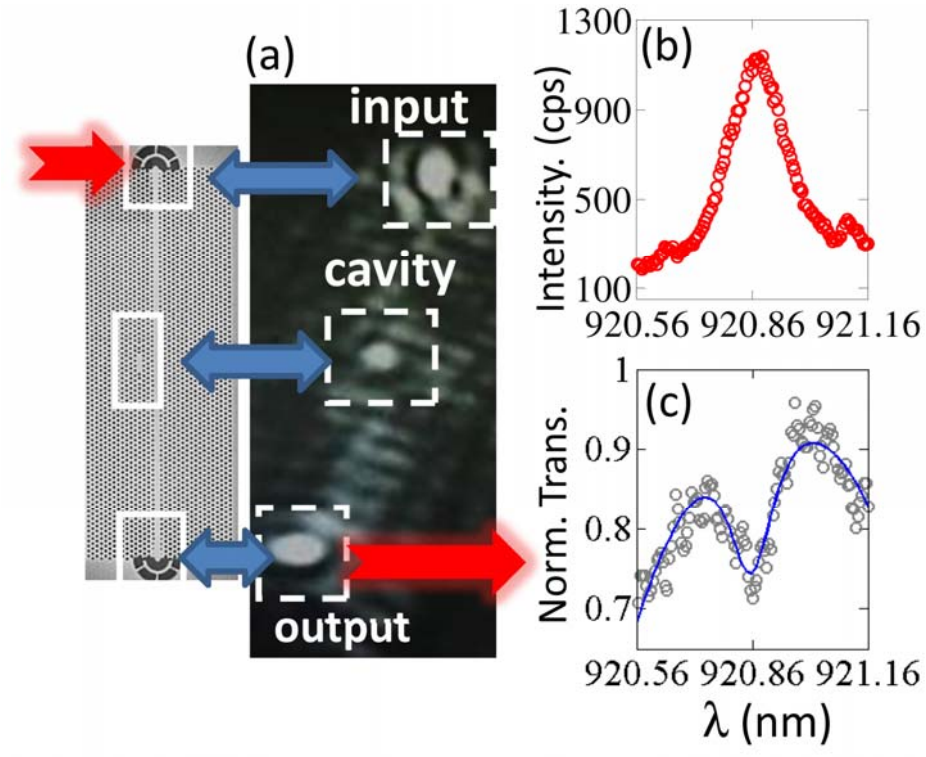

Fig. 4. (a) CCD image of the device under laser excitation showing radiation at the input and output gratings as well as the cavity region when the laser is tuned to the resonance of the cavity mode. An SEM of the typical device is also shown on the left for reference. (b) Photoluminescence spectrum of the cavity-QD system when the QD is detuned by 0.3 nm from the cavity mode. (c) Transmission measured at the same QD-cavity detuning condition as in (b) showing a dip corresponding to the cavity transmission.

Having characterized the photoluminescence properties of the cavity, we next probe the strongly coupled cavity-QD system through the scattering spectrum of the cavity and transmission spectrum of the waveguide by injecting light into the waveguide through the input grating coupler. Upon irradiating the input grating with a focused light source a clear radiation was observed from both the cavity and the output coupler, as shown in Fig. 4a. This figure shows a CCD image of the device when the input coupler is excited by a narrowband laser source that is tuned to be resonant with the cavity, along with an SEM image of the fabricated structure as a reference. The scattered spot from the cavity and output coupler are indicated, and can be isolated by spatial filtering using a small aperture.

We first considered the emission from the output coupler, which is proportional to the light intensity transmitted through the waveguide, when the QD is not coupled to the cavity. To decouple the two systems we set the sample temperature to 14K where the QD is detuned from the cavity by 0.3 nm. This detuning is larger than the cavity linewidth so the system behaves as a bare cavity evanescently coupled to a waveguide. A PL spectrum obtained using high power above-band excitation at this temperature is shown in Fig. 4b. At these pump powers all QDs saturate and enabling us to clearly isolate the cavity emission which is centered at a wavelength of 920.86 nm.

Figure 4c shows the normalized transmission spectrum of the waveguide, observed by now focusing a broadband LED on the input coupler and collecting emission only from the output coupler using a small aperture. The spectrum of the transmitted light is measured using

#141797 - $15.00 USD Received 27 Jan 2011; accepted 27 Feb 2011; published 8 Mar 2011

the grating spectrometer. The transmission of the waveguide was found to significantly vary with wavelength due to the spectral response of the grating couplers as well as Fabry-Perot fringing effects caused by multiple reflections between the two couplers and the cavity. At the cavity resonance wavelength of 920.86 nm, we observe an anti-resonance in the transmission spectrum superimposed on the broader spectral response of the waveguide. This anti-resonance is due to the evanescent coupling of the cavity mode to the waveguide.

The transmitter power spectrum, denoted $S_T(\omega)$, can be compared to the theoretically predicted value based on cavity input-output formalism [28], which is given by

$$S_T(\omega) = \left|\varepsilon(\omega)\right|^2 \left| \frac{i2\Delta_c + \kappa(1-r_0)}{i2\Delta_c + \kappa} \right|^2 . \qquad (2)$$

Here, $r_0 = 2\kappa_{||}/\kappa$ is the reflectivity of the bare cavity (no QD) on resonance where $\kappa_{||}$ is the decay rate of the cavity into the forward and backward propagating modes of the waveguide, $\Delta_c = \omega - \omega_c$ where ω and ω_c are the driving field frequency and cavity resonant frequency respectively, and $\varepsilon(\omega)$ is the amplitude of the incident driving field. In order to fit the data to the spectrum described in Eq. (2), we need to know the frequency dependence of the input field $\varepsilon(\omega)$, which is very difficult to characterize because it depends on the unknown spectral response of the gratings and Fabry-Perot fringing caused by multiple reflections. To attain an accurate measurement of this response we would need to remove the cavity-QD system and characterize the waveguide and grating couplers alone, something we cannot do. Instead, we perform a second order Taylor series expansion of the field given by $\left|\varepsilon(\omega)\right|^2 = c_0 + c_1(\omega - \omega_c) + c_2(\omega - \omega_c)^2$. The coefficients c_0, c_1, and c_2 are treated as fitting parameters to attain the best match to the experimental data.

Using r_0 and κ as additional fitting parameters, we fit the experimental transmission spectrum to Eq. (2). The best fit, shown as a solid line in Fig. 4c, is attained for $r_0 = 0.12$ and $\kappa = 56$ GHz. From these parameters, we calculate $\kappa_{||}$ to be 3.4 GHz corresponding to $Q_{||} = 95800$. This high value for the planar Q suggests that we are operating in the undercoupled regime. The transmission of the waveguide on resonance is given by $T_c(\omega_c) = (1- r_0)^2 = 0.77$, in close agreement with the theoretical value of 0.71 calculated from FDTD simulations as described in section 2.

The sample temperature was next set to 27 K in order to tune the QD onto resonance with the cavity mode. The broadband diode was once again focused onto the input coupler, and Fig. 5a shows the spectrum from the light directly scattered out of plane by the cavity. This spectrum was obtained by spatially filtering emission scattered from the cavity region and measuring the spectrum using the grating spectrometer. The scattered power spectrum is plotted as a function of detuning between the incident field wavelength λ and the cavity resonant wavelength λ_c. Near the cavity resonance, significant enhancement of the scattered power is observed. However, instead of a single Lorentzian line, a doublet feature is observed in the cavity-radiated emission due to interaction with the strongly coupled QD. The central dip in the normalized scattering spectrum exhibits a peak-to-dip contrast of 49%, which is higher than the contrast of the photoluminescence spectrum at low excitation powers, measured to be 37%. This increased contrast is a manifestation of destructive interference between polariton modes [20].

#141797 - $15.00 USD Received 27 Jan 2011; accepted 27 Feb 2011; published 8 Mar 2011

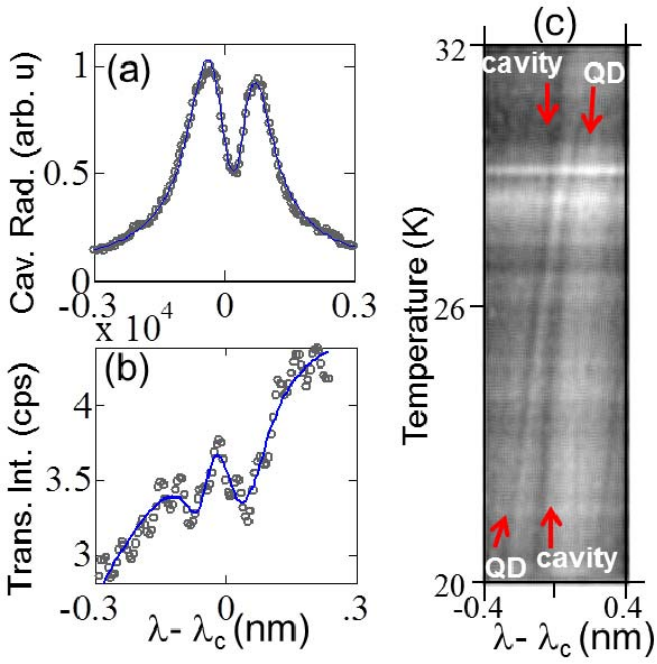

Fig. 5. (a) Scattering spectrum for QD-cavity system in the weak-field condition at 27 K. (b) Transmission spectrum of the cavity-QD system on resonance at 27 K. (c) Transmission measured as a function of temperature between 20- and 32K showing an anti-crossing between the anti-resonances corresponding to the two polaritons.

The measured scattering spectrum can be compared to the theoretical predictions based on a two-level atomic system coupled to a single cavity. The scattering spectrum for such a system has been previously investigated in several works [20,29–31] under the approximation that the atomic system only undergoes decay, but does not experience dephasing. Such approximation is unrealistic for InAs QDs where the coherence time can be significantly shorter than the excited state lifetime [32]. In the presence of dephasing, it has been shown that one cannot simply replace the dipole decay rate, denoted γ_a, by the standard semi-classical expression $\gamma_a = (\gamma_r + \gamma_{nr})/2 + 1/T_2$ where γ_r is the radiative decay rate, γ_{nr} is the non-radiative decay rate, and T_2 is the coherence time [33]. The correct expression for the scattered power spectrum is given by $S_S(\omega) = \eta\kappa_\perp n$ where $\kappa_\perp$ is the out-of-plane cavity decay rate, η is the photon detection efficiency which accounts for the collection optics as well as detector quantum efficiency, and n is the cavity photon number given by [33]:

$$n = \frac{4}{4\Delta_c^2 + \kappa^2}\left(\frac{g^2|\rho_{21}|^2}{\Gamma}\left[\gamma_a + \frac{2g^2\kappa}{4\Delta_c^2 + \kappa} \right] + 2g\sqrt{\kappa}\,\mathrm{Im}\left[\varepsilon^* \rho_{21} \right] + \kappa|\varepsilon|^2 \right). \quad (3)$$

In the above equation γ_a is the previously defined semi-classical dipole decay rate, and $\Gamma = \gamma_r + \gamma_{nr} + 4g^2\kappa/\left(\kappa^2 + 4\delta^2\right)$ is the modified QD decay rate where $\delta = \omega_a - \omega_c$ and ω_a is the QD resonant frequency. The term ρ_{21} is the off diagonal dipole term of the reduced density matrix for the QD which, in the weak field limit, is given by

$$\rho_{21} = \frac{\Omega(i\Delta_c + \kappa/2)}{(i\Delta_a + \gamma_a)(i\Delta_c + \kappa/2) + g^2}, \quad (4)$$

#141797 - $15.00 USD Received 27 Jan 2011; accepted 27 Feb 2011; published 8 Mar 2011

where $\Delta_a = \omega - \omega_a$, and $\Omega = -ig\sqrt{\kappa}\varepsilon/(i\Delta_c + \kappa/2)$. We note that because $\rho_{21} \propto \varepsilon$ we have $n \propto |\varepsilon|^2$ as expected in the weak excitation limit where the system is a linear scatterer and so the scattering rate should be proportional to the input photon flux.

We fit the theoretical model given in Eq. (3) to the experimental data shown in Fig. 5a. The fitting parameters used were g, γ_a, δ, and $s_0 = \eta\kappa_\perp |\varepsilon|^2$, which is the peak scattering rate with no QD. We also treat the spectrometer background level as an additional fitting parameter. The solid line plots the best fit curve to the data, which is attained for the parameter values g = 17 GHz, γ_a = 6.3 GHz, and δ = 3.7GHz.

We next consider the transmission of the waveguide by collecting light at the output port, as shown in Fig. 5b. The transmitted spectrum exhibits an anti-resonant doublet feature, where the minima of the anti-resonances correspond to the peak values of the corresponding resonances in Fig. 5a. This doublet corresponds to mutual scattering from the two polariton modes of the cavity, and is the signature of strong coupling observed through the waveguide transmission.

The experimental measurements for transmission can be compared to the theoretical values which can be also be calculated using cavity input-output formalism [28]. The input-output relation for the cavity is given by $\mathbf{a_{out}} = \varepsilon(\omega) - \sqrt{r_0\kappa/2}\mathbf{a}$ where ε is once again the coherent input driving field amplitude, $\mathbf{a_{out}}$ is the bosonic flux operator for the transmitted field, $\mathbf{a}$ is the bosonic annihilation operator for the cavity mode, and, as before, $r_0 = 2\kappa_{||}/\kappa$ is the reflectivity of the bare cavity (no QD) on resonance where $\kappa_{||}$ is the decay rate of the cavity into the forward and backward propagating modes of the waveguide. The transmitted flux is given by $\langle \mathbf{a}_{\mathbf{out}}^\dagger \mathbf{a}_{\mathbf{out}} \rangle = |\varepsilon(\omega)|^2 - \sqrt{2r_0\kappa}\,\mathrm{Re}\{\varepsilon^*(\omega)A\} + r_0\kappa n/2$, where $A = \langle \mathbf{a} \rangle$ and n is the cavity photon number given in Eq. (2). In the weak field limit we have [33]

$$A = \frac{\sqrt{\kappa}\varepsilon(\omega)(i\Delta_a + \gamma_a)}{(i\Delta_c + \kappa/2)(i\Delta_a + \gamma_a) + g^2}. \tag{5}$$

We again note that in the weak field limit the transmitted power is proportional to $|\varepsilon(\omega)|^2$. As before, we perform a second order Taylor series expansion of the incident field power spectrum given by $|\varepsilon(\omega)|^2 = c_0 + c_1(\omega - \omega_c) + c_2(\omega - \omega_c)^2$. The coefficients c_0, c_1, and c_2 are treated as fitting parameters to attain the best match to the experimental data.

The fitting parameters used to compare experiment to theory are the expansion coefficients for the background, along with g, δ, γ_a, ω_c, and r_0. The solid line in Fig. 5b shows the best fit curve for the data, which is attained for g = 15.8 GHz, δ = –15.2 GHz, γ_a = 7.2 GHz, and r_0 = 0.12. These numbers are consistent with the fitting for the scattered field, and the previously determined parameters using the bare cavity transmission. We note that in the transmission measurement the QD was slightly detuned from the cavity mode, but this detuning was small compared to the cavity linewidth.

In Fig. 5c, we show experimental data from a temperature tuning experiment in which the strongly coupled QD was tuned across the cavity resonance. Here, the transmission of the waveguide was recorded at each temperature using the broadband LED source at the input coupler. At each temperature two anti-resonances can be observed, which correspond to the two polariton modes of the cavity-QD system. As the QD is tuned across the cavity frequency a clear anti-crossing can once again be observed as was shown in Fig. 3a, but this time in the anti-resonances of the waveguide transmission. The minimum splitting between the two anti resonances, achieved at 27 K, is given by 0.1 nm which is consistent with values obtained from the cavity photoluminescence.

#141797 - $15.00 USD Received 27 Jan 2011; accepted 27 Feb 2011; published 8 Mar 2011

6. Waveguide transmission in the strong field limit

The quantum-optical state of the cavity-QD system is strongly intensity dependent. In the weak excitation regime (Fig. 5), the QD predominantly occupies the ground state, and the laser scan in the cavity radiation and transmission measurements show the dressed polariton states. As the excitation power is increased, the exciton becomes saturated and decouples from the cavity. In this limit the power spectrum of the scattered and transmitted fields are expected to approach those of the bare cavity mode.

To perform high power measurements, we measure the cavity spectrum using a tunable narrowband external cavity laser diode. This excitation source can inject high field intensity into a narrow spectral bandwidth in order to strongly excite the QD. The cavity spectrum is obtained by pumping the input coupler and sweeping the laser diode frequency. At each frequency the amount of scattered light is recorded. Figure 6a shows a result of a wavelength sweep for several different excitation powers (5 μW, 60 μW and 90 μW from bottom to top) where we collect the scatter directly from the cavity. At a low pump power of 5 μW the spectrum is nearly identical to the low power spectrum attained by the broadband LED, shown in Fig. 5a. As the pump power is increased to 60 μW the contrast of the central dip is reduced, while at an even higher pump power of 100 μW the central dip is almost completely absent from the spectrum.

A similar behavior can be observed in the waveguide transmission. Figure 6b and 6c plot the light intensity scattered from the output coupler for two different laser powers. Panel b plots the low power spectrum when the pump is set to 5 μW, while panel c plots the high power spectrum taken with a pump power of 125 μW. Once again, at low powers the transmission exhibits two anti-resonances corresponding to the two polaritons. The data is plotted along with the theoretical fit attained by setting g = 15.8 GHz and γ_a = 7.2 GHz, the values obtained by fitting the data in Fig. 5c, while leaving the remaining fitting parameters free. At high power a single resonance corresponding to the cavity mode is observed due to QD saturation. The high power data is also plotted along with the fit to Eq. (2), where best fit value for r_0 is found to be 0.1, consistent with the values obtained from the data in Fig. 4c.

#141797 - $15.00 USD Received 27 Jan 2011; accepted 27 Feb 2011; published 8 Mar 2011

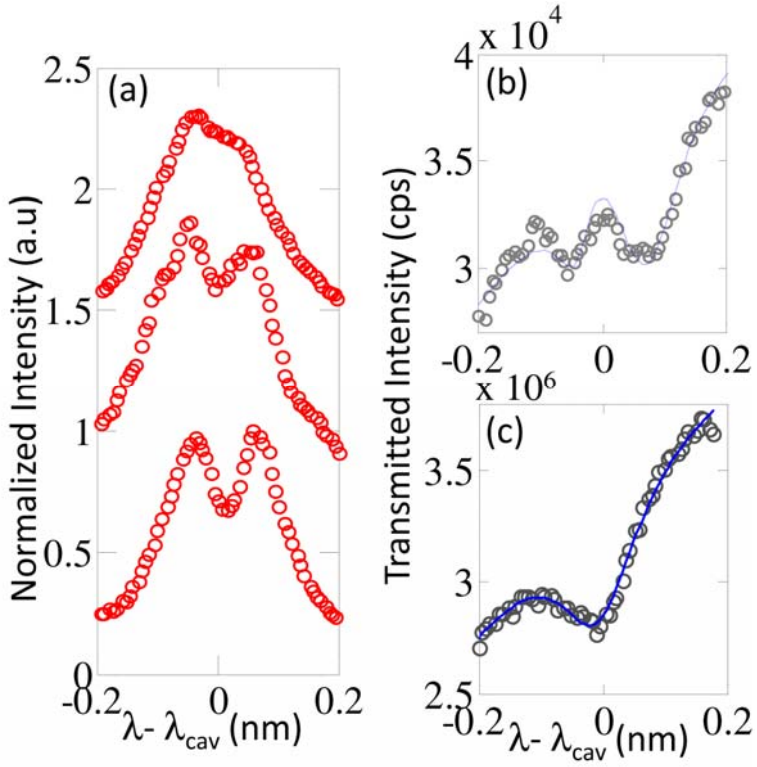

Fig. 6. (a) Cavity emission for increasing excitation powers of the input laser with incident powers, from top to bottom, of 100 μW, 60 μW, and 5 μW. (b) Waveguide transmission measurement at 5 μW. (c) Waveguide transmission at 125 μW. In (b) and (c) fitting curves are shown using solid lines, while the experimental data is shown using circles.

7. Conclusion

In conclusion, we have successfully demonstrated a fully integrated cavity waveguide system where the cavity mode is strongly coupled to a QD. The quantum state of the system is measured using a transmission setup where both input and collection occur away from the cavity region. A 24% reduction in waveguide transmission was observed on cavity resonance due to evanescent interaction between the waveguide and cavity modes. Strong coupling was observed through modification of the transmission of the waveguide resulting in a double anti-resonance at the locations of the two polariton energies. The waveguide transmission was also found to be extremely intensity dependent as expected due to saturation of the QD absorption. Improved devices with better contrast could be attained by using designs that achieve better overlap between the cavity and waveguide mode [34]. These results represent an important step towards complex integrated planar devices where interactions between multiple cavity-QD systems can be achieved using optical channels.

Acknowledgements

The authors acknowledge support from the ARO MURI on hybrid quantum interactions (grant number W911NF09104), the physics frontier center at the Joint Quantum Institute, and the ONR Applied Electromagnetic Center. E. Waks acknowledges support from an NSF CAREER award (grant number ECCS – 0846494). R. Bose and D. Sridharan contributed equally to this work.

#141797 - $15.00 USD Received 27 Jan 2011; accepted 27 Feb 2011; published 8 Mar 2011